On the formation of barrier layers and associated vertical temperature inversions: A focus on the northwestern tropical Atlantic

J. Mignot,[1] A. Lazar,[1] and M. Lacarra[1]

Received 6 July 2011; revised 26 November 2011; accepted 28 November 2011; published 3 February 2012.

[1] A unique barrier layer (BL) system in terms of persistence, extension, and associated subsurface temperature maximum is present seasonally in the northwestern tropical Atlantic. Based on climatological output of a general circulation ocean model, we show here that its development consists of two phases. In summer, the BL is relatively shallow and thin but subsurface temperature maxima are intense. The latter develop as a result of the specific seasonality of the freshwater discharge in this area, which limits the mixed layer to a very thin depth while the intense radiative heat flux penetrates significantly below, thereby heating the subsurface waters protected from air-sea interactions and inducing a barrier layer between the mixed layer and the ocean interior. In winter, the BL development is due to a surface decrease in salinity associated with the surface freshwater capping, which decouples the pycnocline, and hence the winter mixed layer, from the thermocline. The mechanism is ubiquitous in the sense that it is very similar to that of other areas at the same latitude, as well as at high latitudes in regions of seasonal surface freshening. Results are discussed in the light of a simple linear equation linking the BL development to time evolution of Sea Surface Temperature and Sea Surface Salinity stratification.

Citation: Mignot, J., A. Lazar, and M. Lacarra (2012), On the formation of barrier layers and associated vertical temperature inversions: A focus on the northwestern tropical Atlantic, *J. Geophys. Res.*, *117*, C02010, doi:10.1029/2011JC007435.

1. Introduction

[2] The northwestern tropical Atlantic was shown by *Mignot et al.* [2007, hereinafter MBLC07] to be a region with very thick and long lasting barrier layers (BLs). These BLs could furthermore be shown to be particularly persistent and impermeable on monthly timescales as defined by *Mignot et al.* [2009]. Their formation mechanism was studied by *Pailler et al.* [1999], *Masson and Delecluse* [2001], and *Ferry and Reverdin* [2004]. These authors highlighted in particular the influence of outflow from adjacent rivers. Indeed, two of the strongest rivers in the world (namely the Amazon and the Orenoque) outflow in this region, giving rise to a pronounced and specific Sea Surface Salinity (SSS) seasonal cycle. However, these previous studies largely ignored the deep and strong co-localized vertical temperature inversions that exceed 0.6°C [*de Boyer Montégut et al.*, 2007a, hereinafter BMLC07]. The latter are among the most vast, deep and strong of the tropical oceans. The climatic impact of temperature inversions has been illustrated by *Smyth et al.* [1996], *Vialard and Delecluse* [1998], and *Durand et al.* [2004] in the Pacific and in the Indian Ocean. Recently, *Balaguru* [2011] suggested a possible link between BLs and inversions in the tropical Atlantic and tropical cyclones.

[3] The BL system of the northwestern tropical Atlantic (Figure 1 and thick box in Figure 2) is located within the so-called Atlantic Warm Pool (AWP) that occupies the Gulf of Mexico, the Caribbean Sea, and the western tropical North Atlantic. Using atmospheric reanalysis and sensitivity experiments with an atmospheric general circulation model, *Wang et al.* [2006, 2008b] also showed the significant influence of the warm waters in the Atlantic Warm pool on western hemisphere summer rainfall and Atlantic hurricanes. The mechanism involves a modulation of the tropospheric vertical wind shear and thus of the moisture static stability of the overlying atmosphere. *Wang et al.* [2008a] also showed the link between the AWP's multidecadal variability and the larger scale Atlantic Multidecadal Oscillation (AMO) [*Knight et al.*, 2005] suggesting that the influence of the AMO on the tropical Atlantic cyclone activity, illustrated for example by *Enfield and Cid-Serrano* [2010], may operate through the mechanism of AWP-induced atmospheric changes. Furthermore, important interactions between this region and the tropical Pacific occur, in particular in terms of freshwater exchange [e.g., *Giannini et al.*, 2000; *Wang and Enfield*, 2003]. Finally, the BL system of the northwestern tropical Atlantic is located on the path of the surface branch of the Atlantic Meridional Overturning Circulation, so that its formation and seasonality could also be linked to remote oceanic conditions and influence the whole Atlantic climate

[1]UPMC/CNRS/IRD/MNHN IPSL-LOCEAN, Paris, France.

0148-0227/12/2011JC007435

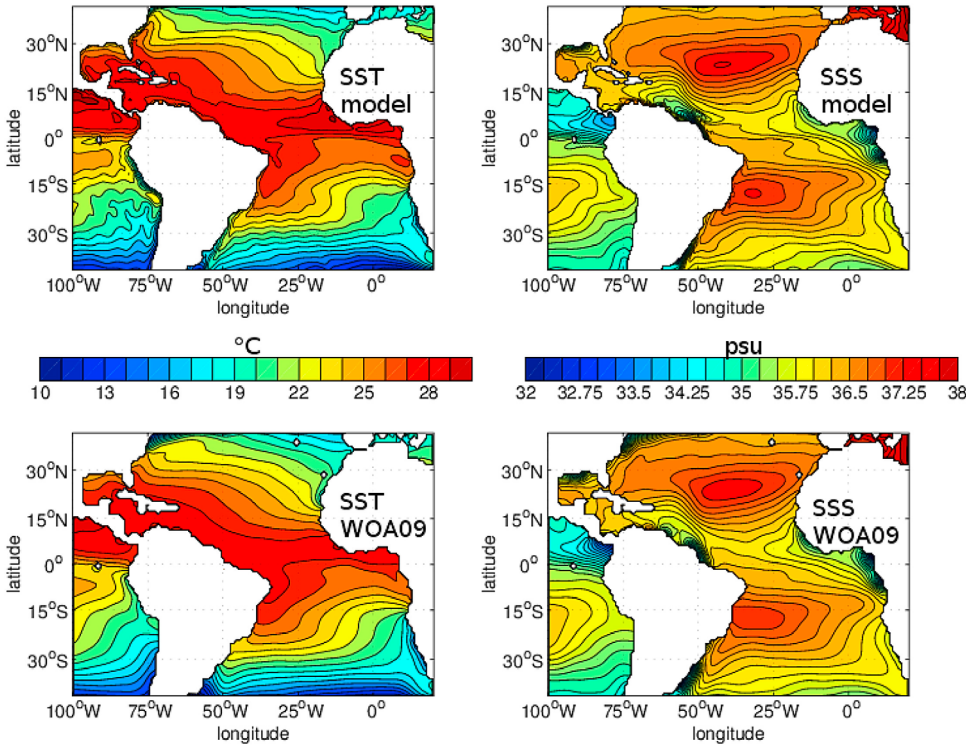

Figure 1. Annual mean (left) sea surface temperature (in °C) and (right) sea surface salinity (in psu) in (top) the simulation and (bottom) the WOA09 data set [*Locarnini et al.*, 2010; *Antonov et al.*, 2010].

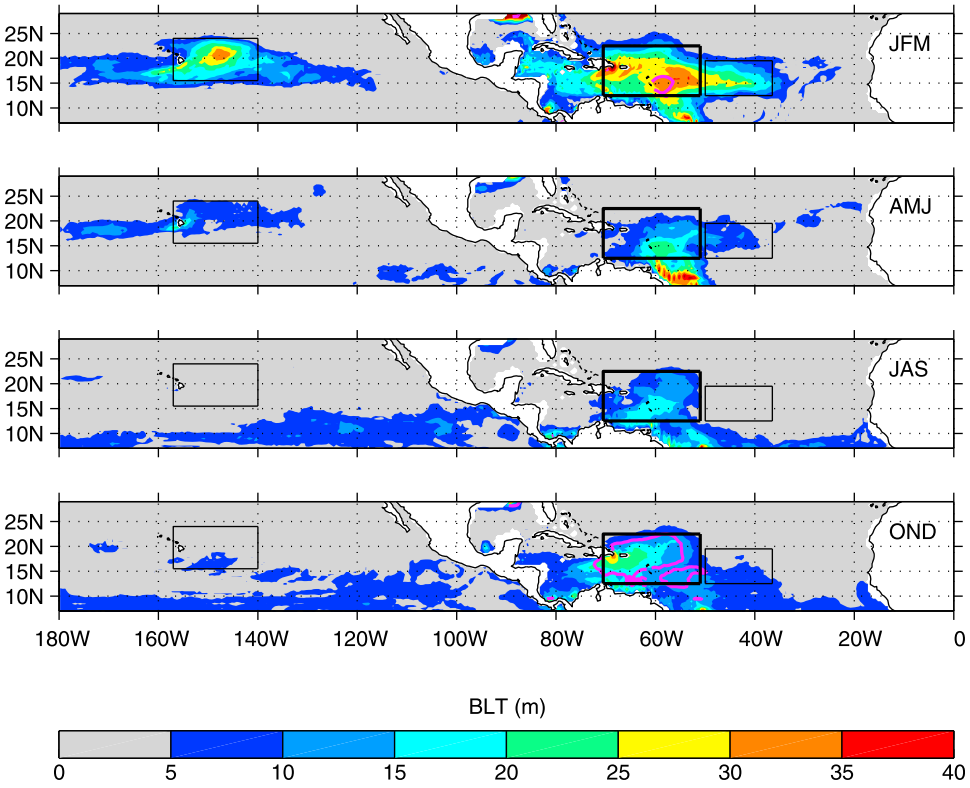

Figure 2. BL thickness (color scale) in the northern tropical Atlantic and east Pacific in the model. The magenta contours are subsurface temperature maximum greater than 0.6°C. The boxes highlight the BLs studied in the rest of the paper.

through oceanic conditions. This location is thus unique in terms of climatic variability and climatic impact.

[4] The studies of BMLC07 and MBLC07 also showed the presence of robust and thick BLs at similar latitudes in the center of each subtropical oceanic basin in winter. For the first time, these studies proposed a symmetry among subtropical oceanic basins in terms of BL climatology and formation processes. As compared to the BL system in the northwestern tropical Atlantic, BLs in the central subtropical basins appear later in the winter season and they are not associated with significant inversions of the vertical temperature gradient. This suggests that BL formation in the western tropical Atlantic may be specific to this region, although this is not well understood yet. In her recent study using sensitivity experiments with a coupled climate model, *Balaguru* [2011] suggested an important role of subsurface salinity for the formation of these BLs and of the surface salinity for the creation of the vertical temperature inversions.

[5] Our objective here is to gain a general understanding of the formation process of BLs and temperature inversions in tropical areas. In particular, a vertical temperature inversion requires a strong salinity stratification in order to keep the water column stable. How does the seasonality of the specific freshwater discharge and precipitation in this area participate in the formation of persistent BLs and strong subsurface temperature maxima? Is the latitudinal symmetry highlighted in MBLC07 still valid for this specific region? In order to address these issues, we propose to compare time series of the BL development in the northwestern tropical Atlantic to that of other subtropical BLs at similar latitudes. We deduce from this analysis that the development of the BL system in the northwestern tropical Atlantic happens in two steps, one due to the specificity of the region and the second similar other BL systems at similar latitudes. We also propose a prognostic equation for the BL development that is, under certain assumptions, applicable to all BL areas. We believe that such a model can be useful to modelers and observationalists to interpret or predict the presence or absence of BLs.

[6] In order to analyze in details the temperature and salinity budgets associated with BLs, we base our study on the outputs of a forced Ocean General Circulation Model (OGCM) The model and BL thickness computation are presented in section 2. The analysis of the BL system, its seasonality and its development mechanism are shown in section 3. In section 4, we derive a simple linear prognostic model for the BL development as a function of temperature and salinity stratifications, and we propose to use it as a framework to illustrate BL developments in the tropical band. Conclusions are given in section 5.

2. Model and Definitions

2.1. The Ocean Circulation Model

[7] We use the global Océan Parallèlisé (OPA) OGCM [*Madec et al.*, 1998]. OPA solves the primitive equations on an Arakawa C grid, with a second-order finite difference scheme. It assumes the Boussinesq and hydrostatic approximations, and the incompressibility hypothesis, and uses a free-surface formulation [*Roullet and Madec*, 2000]. The density is computed from potential temperature, salinity, and pressure using the *Jacket and McDougall* [1995] equation of state. In its global configuration ORCA05, the horizontal mesh is based on a $0.5° \times 0.5°$ Mercator grid, and following *Murray* [1996], two numerical inland poles have been introduced in order to remove the North Pole singularity from the computational domain. The departure from the Mercator grid starts at 20°N and is constructed using a series of embedded ellipses based on the semianalytical method of *Madec and Imbard* [1996]. Realistic bottom topography and coastlines are derived from the study of *Smith and Sandwell* [1997], complemented by the 5′ Gridded Earth Topography (ETOPO5) dataset. The maximum depth of 5000 m is spanned by 30 z-levels ranging from 10 m thickness in the upper 120 m to 500 m thickness at the bottom. The ocean model is run with a time step of 2400 s.

[8] Lateral tracer mixing is done along isopycnals. Eddy-induced tracer advection is parameterized following *Gent and McWilliams* [1990] with coefficients decreased in the Tropics between 20°N and 20°S. Momentum is mixed along horizontal surfaces using coefficients varying with latitude, longitude, and depth. Vertical eddy diffusivity and viscosity coefficients are computed from a 1.5-level turbulent closure scheme based on a prognostic equation for the turbulent kinetic energy [*Blanke and Delecluse*, 1993]. Double diffusive mixing (i.e., salt fingering and diffusive layering) is computed following *Merryfield et al.* [1999]. Penetrative solar radiation corresponding to Type I water [*Jerlov*, 1968] is also used. This formulation will be detailed in section 3.2. This model configuration has been widely used for climatic studies, such as in the study by *de Boyer Montégut et al.* [2007b].

[9] The model run starts from an ocean at rest using the January temperature and salinity fields of the *Levitus* [1998] climatology. It is then run for a 3-yr period using a climatology of 1992–2000 forcing fields. In this study, we focus on climatological BL systems. This was our motivation for choosing this particular set up using a climatological forcing, thereby avoiding the effect of interannual variability and long-term trend. Such a forcing strategy has proven useful for investigating the mean seasonal cycle [e.g., *Durand et al.*, 2007]. Limitations inherent in using climatological values for relative humidity and cloudiness are discussed, for example by *de Boyer Montégut et al.* [2007b].

[10] The momentum surface boundary condition is given using the weekly European Remote Sensing Satellites-1 and -2 (ERS-1-2) wind stress interpolated daily with a cubic spline method [*Bentamy et al.*, 1996]. The insolation, longwave radiation and turbulent heat fluxes (and the evaporation) are computed from the semi-empirical or bulk formulae [*Timmermann et al.*, 2005], which relate the fluxes to the SST (computed by the model) and to meteorological parameters (10-m wind speed, surface air temperature and relative humidity, cloudiness). The daily 2-m air temperature is extracted from the National Centers for Environmental Prediction-National Center for Atmospheric Research (NCEP-NCAR) reanalysis [*Kalnay et al.*, 1996]. Monthly climatologies of relative humidity [*Trenberth et al.*, 1989] and cloudiness [*Berliand and Strokina*, 1980] are used. Precipitation data come from the Climate Prediction Center Merged Analysis of Precipitation (CMAP) product [*Xie and Arkins*, 1997]. The monthly values of river discharge [*United Nations Educational, Scientific and Cultural Organization* (*UNESCO*), 1996] are introduced into the model by

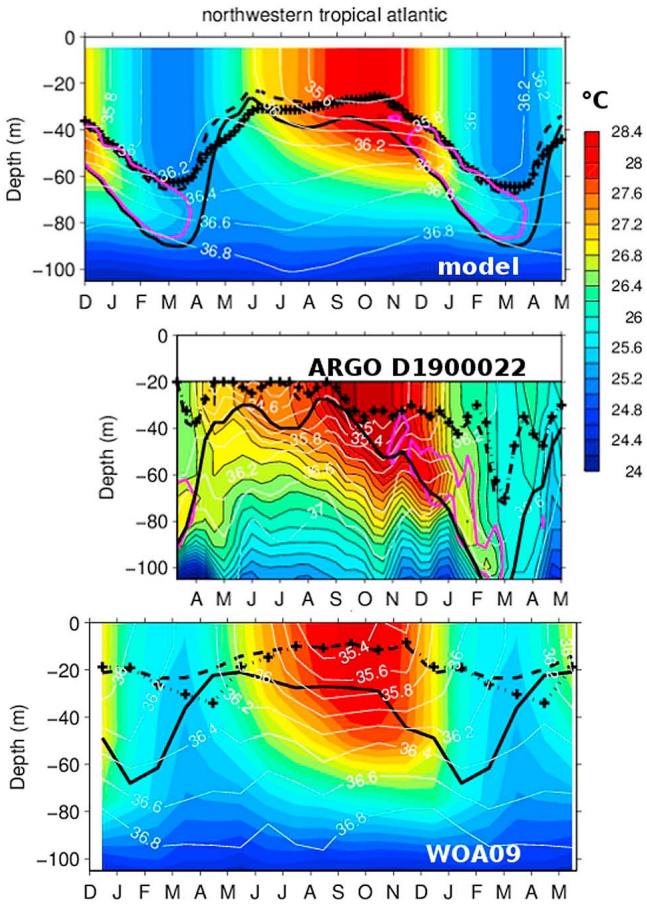

Figure 3. (top) Time evolution of temperature (colors, in °C) and salinity (white contours, in psu) from the surface to 100 m depth averaged over the thick box in the northwestern tropical Atlantic shown in Figure 2. The thick black lines shows the depth D_{T^*-02} (solid), the MLD (dashed) and the halocline depth $D_{S^*+\Delta S}$ with $\Delta S = 0.06$ psu diagnosed from the model data averaged over the same area (crosses). The magenta contour highlights vertical temperature inversions of 0.2° and more. (middle) Time evolution of temperature (colors) and salinity (white contours) from the surface to 100 m depth of the ARGO float D1900022 that traveled in the same area (between 55.5 and 60°W and 14 and 22°N between April 2002 and May 2003). A running mean over 3 points with equal weights has been applied to all time series. (bottom) Same as Figure 3 (top) using the monthly mean temperature and salinity fields from WOA09 [*Locarnini et al.*, 2010; *Antonov et al.*, 2010].

distributing the associated freshwater input as precipitation on the points surrounding the mouth of the rivers. The Amazon runoff is of particular relevance for the present study. Its seasonal variability is well reproduced by the model, as shown for example by *Masson and Delecluse* [2001]. It has a clear annual cycle, with a maximum in May, when it reaches 0.26 Sv, and a minimum in November of 0.13 Sv. A restoring term toward the *Levitus* [1998] SSS is applied to the freshwater budget, with a relaxation timescale of 2 months for a 50-m-thick layer. While there is no physical justification for this feedback term, as the atmosphere does not care about ocean surface salinity, it avoids SSS drift arising from the error in the prescribed freshwater budget.

[11] Available outputs are the temperature and salinity over all the model's vertical levels, as well as tendency terms based on the conservation equations for the temperature and salinity in the mixed layer. Oceanic output are available with 5-days resolution. We use the data from the last year of the model run. Figure 1 illustrates the annual mean SST and SSS fields as given by the model over the Atlantic area (Figure 1, top) and in the most recent version of the World Ocean Atlas (WOA09) [*Locarnini et al.*, 2010; *Antonov et al.*, 2010]. Note that the WOA09 climatology is given with a resolution of 1° only, so that fields appear smoother than in the model. Figure 1 shows that main features of the observed surface fields are quite well reproduced by the model. The SST maximum in the eastern equatorial Atlantic is slightly too warm in the model, and SSS maxima in the subtropics are slightly stronger than in the observations. The validity of this simulation for the BL process studied here will be done below through Figures 2 and 3, presented below.

2.2. Definitions

[12] Following previous barrier layer studies [e.g., *de Boyer Montégut et al.*, 2004], the barrier layer thickness (named simply BLT in the following) is defined here as the difference, when positive, between two depths:

$$BLT = D_\sigma - D_{T^*-02} \tag{1}$$

with $D_{T^*-02} < D_\sigma < 0$. D_{T^*-02} is the depth where the temperature has decreased by 0.2 °C as compared to the temperature at the reference depth of 10 m. The 0.2 °C threshold is based on the current precision of most common temperature sensors. D_σ is the depth where the potential density anomaly, here referred to as σ_θ (potential density $-$ 1000 kg/m^3), has increased from the reference depth by a threshold Δ_σ equivalent to the density difference for the same temperature change at constant salinity:

$$\Delta_\sigma = \sigma_\theta(T^* - 0.2, S^*, P_0) - \sigma_\theta(T^*, S^*, P_0) \tag{2}$$

with T^* and S^* are the temperature and salinity at the reference depth 10 m and P_0 is the pressure at the ocean surface. D_σ corresponds to the top of the pycnocline. Similarly, one can define the halocline depth as the depth where salinity has increased by a threshold ΔS from the reference depth. ΔS is defined such as to induce the same density change as $\Delta T = -0.2$°C. ΔS can thus be estimated from $\Delta S = \alpha_T/\beta_S \times \Delta T$ where α_T and β_S are typical values of the thermal expansion and saline contraction coefficients respectively . With $\alpha_T = 2500 \times 10^{-7}\ K^{-1}$ and $\beta_S = 0.75 \times 10^{-3} psu^{-1}$, we use the threshold $\Delta S = 0.06 psu$ to define the pycnocline.

[13] As shown by *de Boyer Montégut et al.* [2004], in the area of tropical barrier layers examined in the present work, D_{T^*-02} is climatologically deeper than D_σ, and D_σ is a good proxy for the mixed layer depth (MLD), in the sense of a layer where temperature, salinity and density are mixed and thus homogeneous. To the contrary, when D_σ is deeper than D_{T^*-02}, the absolute value of the right hand term in equation (1) gives the thickness of a layer called compensated layer (CL in the following), in reference to a stratification regime where upper halocline and thermocline

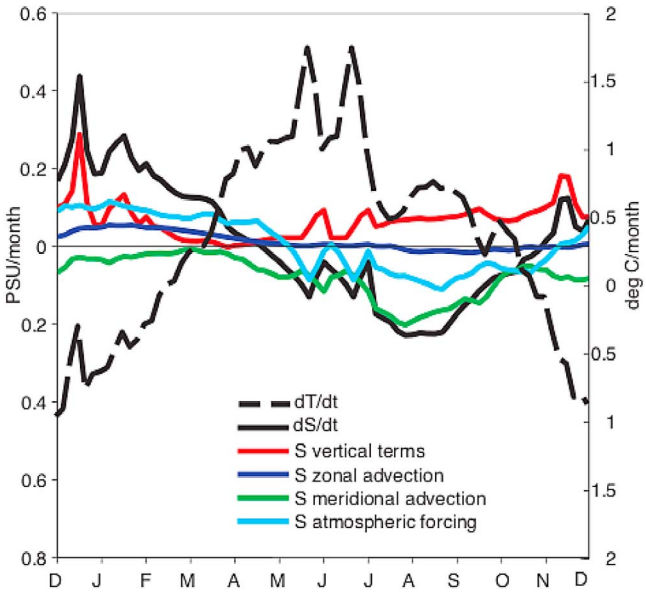

Figure 4. Time series of the mixed layer salinity (thick black line) and temperature (thick dashed line) tendencies computed online by the ocean model averaged over the box shown in Figure 2 with thick lines, in the northwestern tropical Atlantic. For the salinity, the decomposition of this tendency into four physical terms is also shown. The atmospheric forcing term, namely freshwater flux, is in light blue. The zonal advective term ($\vec{u}.\vec{\nabla}S$, where $\vec{u}$ is the zonal velocity) is in dark blue, the meridional advective term ($\vec{v}.\vec{\nabla}S$, where $\vec{v}$ is the meridional velocity) in green. In red, we show the sum of all vertical terms, namely vertical advection, vertical mixing and entrainment. All these terms are computed on-line in the model. The monthly averages that are shown are computed from the 5-days averages available as monthly outputs. The residual between all these terms and the total tendency is small (not shown).

are partially compensated in density. Then, D_σ is no longer a good proxy for the MLD, since it reaches below the top of the thermocline (see *de Boyer Montégut et al.* [2004] for climatological distribution and *Liu et al.* [2009] for interannual variations of the MLD).

[14] Given that in the classic view of a water column, potential temperature is supposed to decrease downward, so that temperature is almost constant above the depth D_{T^*-02}, the latter has been commonly identified in the literature as the Isothermal Layer Depth (ILD). In fact, the layer above D_{T^*-02} is often not isothermal. Instead it may shelter subsurface temperature maxima associated with strong vertical temperature gradients (see BMLC07 for global spatiotemporal distribution of subsurface temperature maxima). Assimilating this surface layer to an ILD overlooks these subsurface temperature inversions that may occur when compensating salinity stratification ensures hydrostatic stability. An important part of the following analysis is precisely dedicated to variations of temperature within this layer and in particular to warming at depth. Therefore, in the following, we prefer to refer to this depth using its definition (D_{T^*-02}) rather than use the misleading acronym ILD. In spite of this ambiguity, this depth, which can be considered as the top of the thermocline, has a clear and important physical definition: it corresponds to the depth below which waters are significantly colder than in surface. By construction, mixing through this interface cools surface waters. In contrast, mixing through the MLD can either warm or cool surface layers, depending on the temperature of waters just below (see Figure 1 of BMLC07 for illustrative hydrological profiles). Note that because subsurface temperature inversions may be present, it is important to consider a decrease of the temperature for the BL definition, whereas an absolute change is used for the temperature mixed layer definition. *Liu et al.* [2009] use an absolute criteria and, as a result, underestimate the BL thickness in cases of temperature inversions.

[15] The time derivative of equation (1) indicates that favorable conditions of BL development occur particularly when D_{T^*-02} becomes deeper, or deepens faster, than the MLD (D_σ). In a cooling season, these conditions are met if a sufficiently strong halocline (with upward decreasing salinity), or a surface salinity decrease, limits the MLD seasonal deepening. In section 4, we will derive equations that help to quantify this consideration and place it in a broader context.

[16] Finally, the temperature inversions are identified, as in BMLC07, by the depth of the subsurface maximum and the difference between this maximum and the temperature of the mixed layer. In this article, we restrict ourselves to temperature inversions located above the thermocline and specifically above D_{T^*-02}.

[17] The computations are done at each spatial grid point of the model, at the temporal resolution of the model output (5 days). Monthly climatologies are then computed as the median of the corresponding 5-day means.

3. Results

3.1. The BL in the Northwestern Tropical Atlantic

[18] Figure 2 shows the seasonal BL thickness in the northern tropical Atlantic and east Pacific basins as well as contours of subsurface temperature maxima. Thick BLs in the northwestern tropical Atlantic, north of the Amazon mouth and east of the Puerto Rico Islands are clearly seen, and are associated with strong vertical temperature maxima (thick box). They compare well with observations shown in MBLC07 (their Figures 1 and 4), although thicknesses are slightly smaller in the model. Vertical temperature inversions are stronger and deeper. This barrier layer system persists roughly all yearlong and reaches its maximum thickness in winter. Vertical temperature inversions are strongest in autumn. The seasonality, longitudinal location and temperature inversion distinguishes this system from BLs located around the same latitudes but in the center of the basins. In the central tropical Pacific and central tropical Atlantic, a thick BL is centered near 20°N and 15°N, respectively, from January to March (thin boxes), consistent with in-situ previous observations (MBLC07).

[19] The time series of modeled temperature and salinity averaged over the area limited by the thick box in Figure 2 and as a function of depth helps in gaining understanding of the evolution of this BL system (Figure 3, top): starting in June from a situation of basic stratification, the salinity stratification strengthens and a BL of about 10 m develops quickly. This formation is due to a quasi-constant mixed layer depth (dashed line in Figure 3 (top)) associated with an

initial deepening of D_{T^*-02} (solid line). Note that mathematically, for a simplified water column with negligible subsurface heat fluxes, D_{T^*-02} is, by construction, expected to shoal between June and October, since the surface temperature warms. This surprising deepening will be analyzed below by considering the effect of penetrating solar radiation. This phase lasts until mid-October, when SST stops warming. The second phase of the BL development starts in early November, when the mixed layer begins to cool and freshen. Both D_{T^*-02} and MLD increase, but at different rates. As a result, the BL deepens down to 80 m and thickens, reaching 20 m. Simultaneously, the temperature inversion appears and develops, occupying the whole BL. It rapidly reaches about 0.4°C. Around April, during the spring restratification, the BL and temperature inversion disappear within 1 to 2 months and both D_{T^*-02} and MLD rapidly shoal back to 40 m depth.

[20] As indicated above, the BL climatology in the model is highly comparable to observations from MBLC07. Nevertheless, before analyzing in detail the BL and temperature inversion evolutions, we can further validate this timing. For comparison, Figure 3 (middle) shows the temperature and salinity measured in the same area between April 2002 and May 2003 by the ARGO float D1900022. Beginning in early May 2002, there is a relatively thin BL around 20 m depth, which persists until August. This BL then deepens and thickens from September onward. A subsurface temperature maximum of 0.1 to 0.2°C is present in mid-June and of more than 0.4°C from October onward. During the autumn and winter, it weakens and deepens with the BL. The BL persists until March, when it was detected around 80 m depth in 2003 and 100 m depth in 2004. This behavior bears strong similarity with the BL development in the model (Figure 3, top). The main difference is that the freshening and the halocline shallowing happens much more quickly in the ARGO float. Furthermore, the minimum thickness observed in August is not seen in the model. However, note that the model results (Figure 3, top) have been spatially averaged over a relatively large area (see box in Figure 2), while Figure 3 (bottom) shows the measurements of a single ARGO float. When model data are averaged over a smaller box restricted to the area spanned by the ARGO float, the spring freshening in particular is much more abrupt and closer to the ARGO measurements (not shown). Furthermore, because the run only shows the climatological variations and the ARGO float takes measurements during a particular year, interannual variability of salinity or temperature, via advection or atmospheric forcing in particular, could also explain part of the discrepancy. Figure 3 (bottom) shows the time evolution and temperature and salinity over the northwestern tropical Atlantic box in the WOA09 [*Locarnini et al.*, 2010; *Antonov et al.*, 2010]. As indicated above, the spatial resolution of this data set is twice that of the model, and the data are only available at monthly time steps. It is thus not suited for a precise analysis of the BL development and we only show it in order to validate the seasonal cycle of temperature and salinity in the area. Indeed, this panel largely confirms the climatological persistence of the BL over the whole year, and the two distinct seasonal patterns: a BL at relatively constant depth in summer, and sudden deepening and thickening in winter.

[21] The overall good agreement between the model and observations gives confidence for using the model to more carefully examine the development of the BL and the subsurface temperature inversion. In particular, it confirms that the two seasons can be analyzed separately: the summer (and surface warming) season, lasting from June to mid-October, when the BL develops as a result of a deepening of D_{T^*-02} while MLD is near constant, and the inter season, from mid-October to early May, when both D_{T^*-02} and MLD deepen, the temperature inversion is much weaker and the BL is thicker.

3.2. The Summer BL

[22] As discussed above, BLs and temperature inversions depend upon the presence of both a salinity and temperature stratification. The model salinity budget in the mixed layer (Figure 4) indicates that the freshening that occurs from April to October is primarily due to meridional advection of freshwater. The dominant freshwater input is thus due to the advection from the equatorward salinity minimum sustained by the Amazon river outflow (maximum in May–June [*UNESCO*, 1996]), and the inter tropical convergence zone (ITCZ, located around 5 to 8°N in August–September). The Amazon outflow peaks to about 0.25 Sv in May, which converts to a trend of roughly 0.75psu/month at the mouth of the river. Observations from *Xie and Arkins* [1997] suggest that local precipitation amounts to about 4mm/day in this region in this season. This corresponds to a salinity trend of about 0.14 psu/month over a mixed layer of 30 m, which is consistent with the model atmospheric forcing term (light blue).

[23] In summer, the mixed layer is maintained at a quasi-constant depth (Figure 3) as a result of the competitive action between surface freshening and warming on the one hand, and vertical mixing due to wind stirring and vertical entrainment on the other hand. The causes, then, of the initial deepening of D_{T^*-02} in June are related to the more general question of what controls the temperature increase below the mixed layer. Since the mixed layer temperature increases during June, the only way D_{T^*-02} can deepen is in case of a faster warming below the MLD, as seen in Figure 3 between 30 m and D_{T^*-02}. The quasi-vertical isotherms visible there in the model, and to a lesser extent in the observations, suggest that the subsurface warming is due to residual vertical turbulence that extends the mixed layer water temperature down to below the mixed layer. However, as detailed below, we argue the penetrative solar radiation explains the evolution of the upper thermocline stratification.

[24] In the model, the solar radiation is allowed to penetrate through the top few meters of the ocean, as described in section 2. To achieve this, a formulation including extinction coefficients is assumed for the downward irradiance I following *Paulson and Simpson* [1977]:

$$I(z) = Q_{sr}\left(Re^{-z\xi 1} + (1-R)e^{-z\xi 2}\right) \tag{3}$$

where Q_{sr} is the penetrative part of the surface heat flux, $\xi 1$ and $\xi 2$ are two extinction length scales and R determines the relative contribution of the two terms. The default values used correspond to a Type I water in the work by *Jerlov* [1968] classification: $\xi 1 = 0.35\ m$, $\xi 2 = 23\ m$ and $R = 0.58$. The contribution of this penetrative radiative flux to the temperature tendency occurs through its vertical derivative following $H = 1/(\rho Cpdz) * (I(k) - I(k+1))$, where dz is the thickness of layer k. Figure 5 (colors) shows this

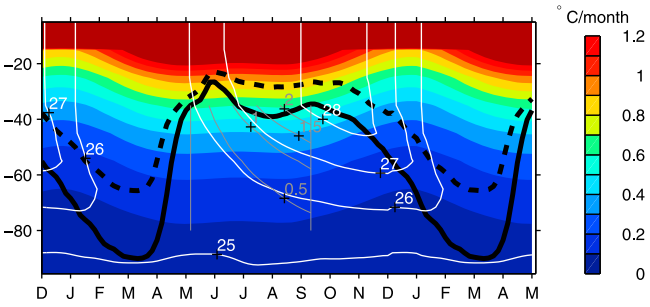

Figure 5. Time evolution of the vertical derivative of the solar penetrative heat flux, expressed in °C/*month* and averaged over the BL area in the northwestern Atlantic (box in Figure 2). For clarity, values above 1.2 °C/*month* and for depths above 15m were not plotted. The thick black lines show the depth D_{T^*-02} (solid), the MLD (dashed) respectively. White contours are temperature contours. The thin grey lines show the temperature change (in °C) due to the cumulative time integration of the penetrative heat flux (colors) from early May to September (vertical thin lines). See text for details.

contribution, which was computed offline as described above. In spring and summer, when the incoming solar flux is maximum, the penetrative flux can reach 0.8°C/*month* at the base of the MLD near 30 *m* and 0.5°C/*month* near 40 *m*. The subsurface warming due precisely to the penetrative heat flux can be quantified by the cumulative time integral of this flux. Thin grey contours in Figure 5 show this integration beginning in early May, when the temperature at 40 m depth is 25.9°C. The grey contours show that at 40 m depth, the penetrative heat flux has induced a warming of 1°C by mid-July, which is consistent with the warming of about 0.9°C seen in the model. This analysis demonstrates the dominant role of penetrative heat flux in subsurface warming, though subsurface mixing and diffusion may compensate at times.

[25] Between July and October, the penetrative flux is around 0.6°C/*month* just below the MLD, which is consistent with the simultaneous subsurface temperature increase from 27.0°C to 28.6°C (colors in Figure 3 (top)). This value exceeds the surface warming rate (less than 0.5°C/*month*; Figure 4, dashed line), so that as the vertical temperature evolves, the isotherms become more vertical and D_{T^*-02} deepens. Meanwhile, the surface advection of low salinity water prevents D_σ from deepening, so a BL forms. Note that the surface warming reaches a relative minimum value in July, further strengthening the relative importance of subsurface warming and favoring the deepening of D_{T^*-02}. In August, as this process persists, the isotherms bend, forming a modest temperature inversion (Figure 3, top) that is permitted by the pre-existing fresh water cap. In agreement with findings of *Vialard and Delecluse* [1998] in the Pacific warm pool, this suggests that the penetrative heat flux is responsible for the observed North Western tropical Atlantic BL and temperature inversion in spring and summer, when the surface freshening maintains a shallow MLD and prevents vertical mixing.

[26] Comparing the summertime dynamics of the northwestern tropical Atlantic to the summertime dynamics of the central Atlantic and Pacific (Figure 6) confirms that it is the specific phasing of the freshening and the maximum solar forcing that permits the summer BL described above to form in northwestern tropical Atlantic. In the central basins, in contrast, the surface warming is rather accompanied by surface salinification (Figure 6) (see also *Dessier and Donguy* [1994] and *Foltz and McPhaden* [2008] for a precise analysis of the SSS seasonal cycle in the Atlantic). As a result, during the summertime warming, the halocline shoals slightly, but remains coupled to the mixed layer depth, so a BL does not form.

3.3. The Winter BL

[27] As described above, at the beginning of winter, the BL development in the northwestern tropical Atlantic clearly enters a second phase (Figure 3) when it deepens and is accompanied by a mixed layer cooling. Figure 6 shows that this second phase occurs also at similar latitudes in the central Pacific (Figure 6, top) and the central Atlantic (Figure 6, bottom). In these two areas, there was no significant source of freshwater to create favorable conditions for a BL formation in summer. Instead, a strong surface freshening occurs in early winter due to the meridional advection of freshwater from the equator by seasonal Ekman transport, as detailed in MBLC07. In the central Atlantic box, the surface freshening occurs from late summer to winter (Figure 6, bottom). In summer, surface temperature is increasing so the freshening is not strong enough to sustain a significant BL. The wintertime freshening, observed in both

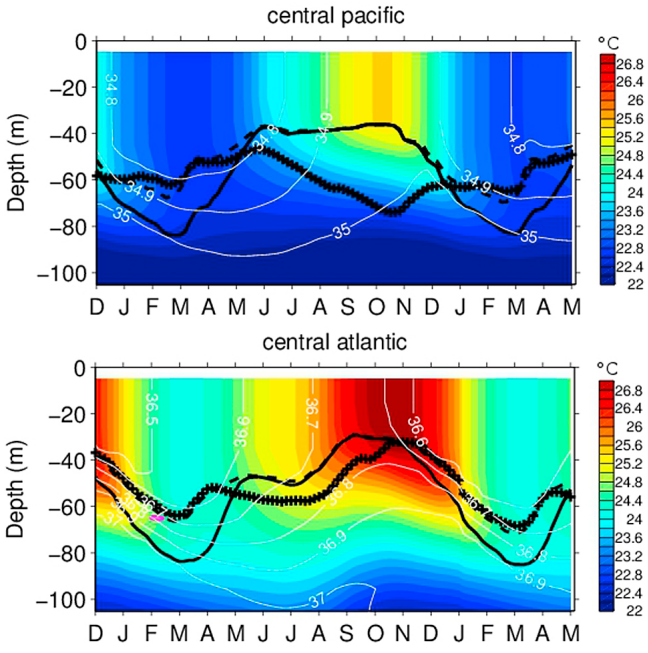

Figure 6. Time evolution of temperature (colors) and salinity (white contours) from the surface to 100 m depth averaged in the (top) central Pacific and (bottom) central Atlantic (see boxes in Figure 2). The thick black lines show the D_{T^*-02} (solid), the MLD (dashed) diagnosed from the model data averaged over the same area. The lines marked with crosses show the depth where salinity is changed by 0.06 psu as compared to the surface value.

the central and northwestern Atlantic, associated with the poleward freshwater advection (MBLC07) can induce a BL that deepens with time. MBLC07 suggested that the BL formation in this area is due to the different response of density (dominated by salinity) and temperature to winter forcing, and in particular to vertical mixing. The analysis of the time series in Figures 3 and 6 clarifies this view: the deepening of D_{T^*-02} is by definition associated with the surface temperature decrease. The deepening of the MLD is due to convective mixing forced by the surface cooling and salinification, as well as the intensification of vertical mixing through an input of momentum from the winds. Again, if salinity was vertically uniform, MLD would equal D_{T^*-02} and neither a BL nor a temperature inversion would appear. Here, the presence of a halocline with a downward gradient is a sufficient condition for a slower deepening of the D_σ, and the BL develops. In the other basins, the phenomenon is similar. A weak vertical temperature inversion (less than 0.1°C) is also associated with the BL due to the fact that the autumn thermocline waters are protected from air-sea interactions and thus cool at a slower rate than the surface waters. Finally, note that in all cases, even though the incoming solar radiative flux is weaker than in summer and the mixed layer is deeper, the penetrative heat flux still has the capacity to heat the layers below the mixed layer (Figure 5) and thus probably helps maintain warm waters below the mixed layer.

4. A Linear Model for the BL Evolution

4.1. A Linear Equation for the BL Evolution

[28] We propose here to derive a simple prognostic equation for the BL thickness (and for the compensated layer, CL, thickness), in order to express the tendency of these layers to form and vanish as a function of temperature and salinity. In the idealized case of a water column with negligible subsurface heat fluxes right below the mixed layer, in the vicinity of D_{T^*-02}, a temporal equation for D_{T^*-02} is:

$$\partial_t D_{T^*-02} = (\partial_z T)^{-1}|_{D_{T^*-02}} \times \partial_t SST, \tag{4}$$

where the vertical temperature gradient is computed at the depth D_{T^*-02}. Equation (4) shows that, for such an adiabatic evolution of the thermocline, and in particular with a standard upward temperature gradient in the thermocline ($\partial_z T < 0$), D_{T^*-02} shoals (respectively deepens) by construction when the SST warms up (respectively cools down). Note that this equation holds in the presence of a subsurface temperature inversion, as long as it is well formed and in a quasi-stationary state. Qualitatively, a relatively strong subsurface warming, as compared to the SST warming, can result in a deepening of the thermocline isotherms with negligible MLD change, leading to a BL thickening. This situation occurs particularly in the tropics in the summer season when $D_{T^*-0.2}$ is closest to the surface and exposed to significant solar penetrative radiations. Mathematically, a corresponding second term should then be added to equation (4).

[29] Following equation (4) and similarly neglecting subsurface buoyancy fluxes near D_σ, one can derive the following equation for the temporal evolution of the pycnocline depth,

$$\partial_t D_\sigma = (\partial_z \sigma)^{-1}|_{D_\sigma} \partial_t SS\sigma, \tag{5}$$

Where $SS\sigma$ refers to the sea surface density. It is then useful to linearize the equation of state according to:

$$\sigma = \rho_{ref}(-\alpha_T T + \beta_S S) \tag{6}$$

with α_T the thermal expansion coefficient of water (neglecting its pressure dependence) and β_S the haline contraction coefficient. Inserting the linearized σ in equation (5) and using equation (1), the time evolution of BLT can be written

$$\partial_t BLT = \frac{-\alpha_T \partial_t SST + \beta_S \partial_t SSS}{-\alpha_T \partial_z T + \beta_S \partial_z S} - \partial_t D_{T^*-02}, \tag{7}$$

where the vertical derivatives are taken at the pycnocline depth. This equation is not valid in the upper ocean where both temperature and salinity are well mixed.

[30] We now introduce the vertical density ratio $R_z = \frac{\alpha_T \partial_z T}{\beta_S \partial_z S}$. R_z is generally similar to R_l, the lateral density ratio [e.g., *Rudnick and Martin*, 2002], which varies significantly over the world oceans between -10 and 10 [*Chen*, 1995].

[31] Using equation (7) and the vertical density ratio, and neglecting the variations over depth of temperature and density vertical gradients, one finally gets

$$\partial_t BLT = \frac{1}{1 - R_z}\left(\frac{\partial_t SSS}{\partial_z S} - \frac{\partial_t SST}{\partial_z T}\right) \tag{8}$$

for $\partial_z S$ and $\partial_z T$ different from zero. Equation (8) is interesting because it indicates that for given vertical temperature and salinity gradients, the BL development depends linearly upon SSS and SST time derivatives. Note that the above hypotheses on temperature and density subsurface fluxes and density linearity imply that subsurface salinity fluxes are also negligible. This last hypothesis is more robust than the one for heat fluxes.

[32] In order to further clarify the role of salinity versus temperature stratification in the development of a BL, one can write a similar equation as equation (4) for $D_{S^*+\Delta S}$:

$$\partial_t D_{S^*+\Delta S} = (\partial_z S)^{-1}|_{D_{S^*+\Delta S}} \partial_t SSS. \tag{9}$$

Then, neglecting the vertical variation of the salinity vertical gradient, equation (7) becomes

$$\partial_t BLT = \frac{1}{1 - R_z}(\partial_t D_{S^*+\Delta S} - \partial_t D_{T^*-02}) \tag{10}$$

This equation indicates that the BL development depends on the evolution of the distance between the top of the thermocline and of the halocline respectively. Hence one can verify that a BL tends to develop if $D_{T^*-0.2}$ deepens faster than $D_{S^*+\Delta S}$, since the latter will limit the deepening trend of D_σ. Figure 7 shows a sketch of the main types of idealized stable vertical profiles of temperature and salinity below the MLD, as in the work by *Liu et al.* [2009]. Note that the latter study related these profiles to the Turner Angle, which is closely related to R_z. Here, it is simpler to relate the profiles directly to R_z as it is the latter that appears in equation (8). The simplest, and most common, case of vertical stratification in the upper ocean corresponds to an upward temperature gradient below the thermocline and a downward salinity gradient below the halocline. In this case, $R_z < 0$ at the base of the thermocline. For $R_z \ll -1$, the temperature gradient

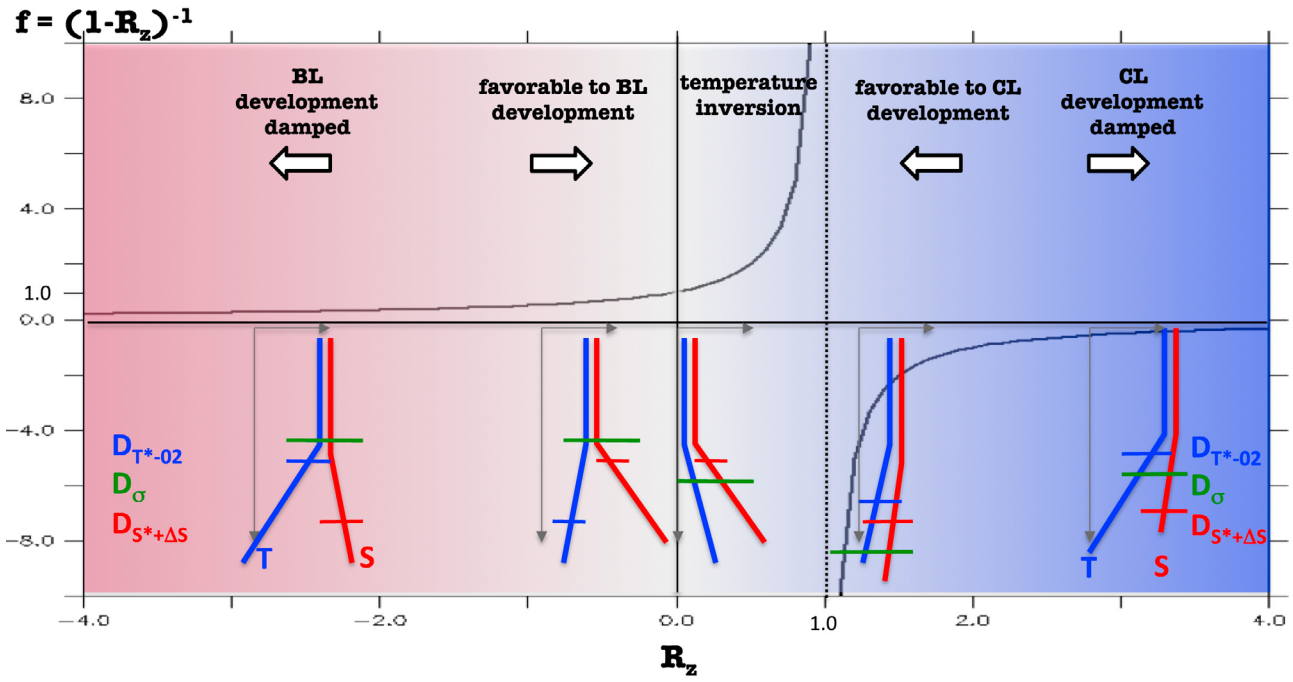

Figure 7. Schematic of the different stratification regimes described in section 4 and link to BL development conditions. The profile graphics illustrate typical temperature (in blue), salinity (in red) profiles as a function of R_z. Horizontal lines on the profiles sketch the D_{T^*-02} (in blue), $D_{S^*+\Delta S}$ (in red) and D_σ (in green) (see text for definitions). The background graphics shows the function $f = (1 - R_z)^{-1}$, which is the modulating factor in equations (8) and (10).

largely dominates the salinity in terms of its effect on the density gradient, and $1/(1 - R_z)$ tends toward zero and damps BL development in equation (10). In other words, D_σ varies almost like $D_{T^*-0.2}$, at the expense of BL development. For R_z close to zero and negative, the salinity gradient now dominates the temperature one, $1/(1 - R_z)$ is close to unity and BL varies in unity with changes in $D_{S^*+\Delta S} - D_{T^*-0.2}$. Such a profile corresponds mainly to weak temperature and strong salinity gradients. In this case, the BL develops essentially because $D_{T^*-0.2}$ deepens easily while D_σ varies almost like $D_{S^*+\Delta S}$, that is little since the halocline is strong (see equation (8)). For $0 < R_z <= 1$, a temperature inversion prevails and density is compensated by a salinity increase. However, equations (8) and (10) do not hold since D_{T^*-02} is not present in such an idealized profile. Another equation for the development of a CL should be derived, but this is beyond the scope of the present study. Note nevertheless that the temperature decreases at greater depth and a thick BL could be defined, as discussed by *de Boyer Montégut et al.* [2007a]. For $R_z >= 1$, the temperature profile is stable and compensated. Equation (10) functions as for the latter regime: $D_{T^*-0.2} > D_{S^*+\Delta S} > D_\sigma$ and $(1 - R_z)^{-1}$ reach high negative values, and a small deepening of $D_{T^*-0.2}$ is, as expected, highly favorable to the development of a CL. Finally, for R_z much larger than 1, profiles are not compensated and the density gradient is controlled by the temperature gradient. Equation (8) says that the changes in CL tends toward zero when R_z grows, in agreement with the lack of compensations. We illustrate below how this equation helps interpreting the tropical BL.

4.2. Interpretation of the Northwestern Tropical Atlantic BLs

[33] Figure 8 shows the values of R_z averaged over the northwestern tropical Atlantic (Figure 8, top) and in the central Atlantic and Pacific basins (Figures 8 (middle) and 8 (bottom), respectively). As discussed earlier, equation (4) is missing an important term of subsurface heat flux, and thus it doesn't explain the evolution of $D_{T^*-0.2}$ in summer in the North Atlantic Warm Pool. In terms of stratification regimes, nevertheless, Figure 8 shows that $-1 \ll R_z < 0$ during this season. The BL modulating factor is then close to unity, and equation (10) confirms that such a situation is favorable to the development of a BL (Figure 7), whose thickness is proportional to changes in the distance separating the top of the thermocline and halocline.

[34] In the central Pacific and Atlantic basins (Figures 8 (middle) and 8 (bottom)), on the contrary, in summer, $D_{S^*+\Delta S}$ is relatively deep (see crosses in Figure 6) while $D_{T^*-0.2}$. is stable or tends to shoal (solid black lines in Figure 6), due to intense surface warming. Hence R_z is strongly negative, and $1/(1 - R_z)$ is close to 0. According to equation (10), this limits BL formation. This is in agreement with the vanishing of the BL that exists in spring prior to the surface salinity decrease (e.g., Figure 3).

[35] In autumn, the rapid weakening of $\partial T/\partial z$ due to surface cooling reduces (in absolute values) R_z, which can eventually even become positive in case of a temperature inversion. Even though equation (4) does not hold in that case, one can see that the modulating factor in equation (10) approaches 1. BLT time variation depends essentially on the

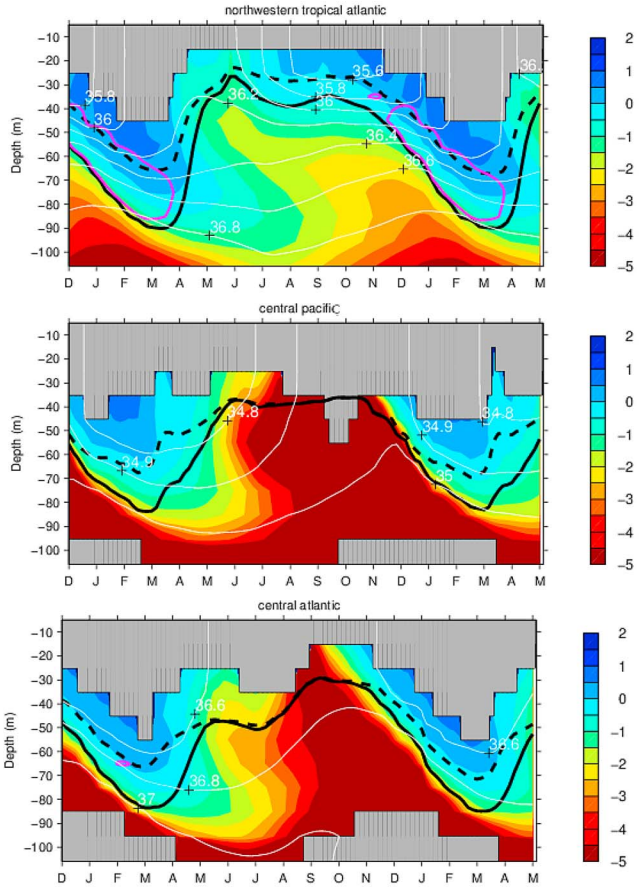

Figure 8. Vertical density ratio $R_z = \frac{\alpha_T \partial_z T}{\beta_S \partial_z S}$ averaged (top) over the present study area and over the (middle) central Pacific area and (bottom) central Atlantic area. Areas where $\partial_z S = 0$ are shown in grey. As in Figure 3, the thick black lines show the depth D_{T^*-02} (solid) and the MLD (dashed) diagnosed from the model data averaged over the same area.

change in distance between the tops of the halocline and the thermocline. $D_{T^*-0.2}$ deepens slightly faster than $D_{S^*+\Delta S}$, and consequently the BL thickens. This holds both in the western tropical Atlantic and in the central basins (Figure 8).

5. Conclusions

[36] We have investigated the formation mechanism of particularly thick and long lasting BLs located in the northwestern tropical Atlantic. The particular motivation was to understand their specific vertical thermal structure as compared to BLs located at the same latitude in the central Atlantic and in the central Pacific: subsurface temperature maxima of up to 1°C can be found in the northwestern tropical Atlantic. This is much more than in any other tropical area of the world, and it extends over a large region.

[37] We have shown that the seasonal cycle of BLs in the northwestern tropical Atlantic is composed of two phases. In spring and summer, intense freshwater input from the Amazon discharge and ITCZ precipitation induce a shallow and strongly marked salinity stratification that limits the deepening of the mixed layer. Meanwhile, some of the intense solar radiative flux penetrates below the mixed layer, inducing the development of unique subsurface temperature maxima and BLs. We argue that in the northwestern tropical Atlantic, the summer BL develops while the mixed layer is maintained at constant depth and the thermocline deepens although the surface temperature increases. In the center of the tropical basins, no major freshwater input such as the Amazon and the Orenoque can decouple the vertical stratification of temperature and salinity during this season and thus prevents a BL from forming during the summer.

[38] In winter, the surface temperature cools and the salinity stratification is maintained through the poleward transport of fresh equatorial mixed layers. The wind-induced mixing leads to a deepening of both the MLD and D_{T^*-02}, but because of the salinity stratification, the two deepen at different rates and a BL is maintained in-between. This second phase of BL development leads to a deeper and thicker BL than during the summer phase. Similar BL development is seen in the central Atlantic and central Pacific. In all three areas, it is associated with a relatively warm reservoir in the BL. The latter is much stronger in the northwestern tropical Atlantic since it results partly from the persistence of the one created in summer. The present analysis, which uses a consistent set of temperature and salinity vertical profiles from model outputs, gives confidence to the winter BL formation mechanism proposed by MBLC07.

[39] These results shade light on the presence of intense subsurface temperature maxima in the northwestern tropical Atlantic. They are indeed due to an early (in terms of seasonality) capping of surface mixing by freshwater input, while the mixed layer is sufficiently shallow to allow significant penetration of radiative heat flux. When the freshwater capping occurs in winter, as in the center of the basins, the mixed layer is already relatively deep and the BL simply occurs as a result of different deepening speed of MLD and D_{T^*-02}. This mechanism is largely consistent with results from model sensitivity experiment performed by *Balaguru* [2011], who also emphasized the importance of surface salinity in the creation of the strong vertical temperature inversions. As indicated in the introduction, previous studies have illustrated the climatic impact of temperature inversions in the Indian and Pacific Ocean. These studies dealt with subsurface temperature exceeding by 0.1 to 0.2°C the surface temperature. Here, the subsurface warm reservoir can exceed the surface temperature by almost 1°C. Its potential impact in terms of tropical cyclone predictability has already been suggested by *Balaguru* [2011]. In the future, we wish to assess the question of potential climatic impact of changes in seasonality and/or magnitude of the Amazon discharge. The mechanism that we purpose here would need to be confirmed by the other high resolution OGCMs, including those under inter-annual forcing.

[40] We have also derived a linear prognostic model for the BL and CL development as a function of temperature and salinity stratifications. We have illustrated that despite strong assumptions, it constitutes a good framework to discuss BL developments, and compare the behavior in different basins or seasons. The numerous possible improvements of this model, such as the inclusion of subsurface heat fluxes, are left for future studies.

[41] **Acknowledgments.** We would like to thank Nicolas Martin for help with the ARGO floats. The authors also acknowledge Christian Ethé

for the simulation. We also acknowledge Kyla Drushka and the editor for useful and constructive remarks that greatly helped to improve the manuscript.

References

Antonov, J. I., D. Seidov, T. P. Boyer, R. A. Locarnini, A. V. Mishonov, H. E. Garcia, O. K. Baranova, M. M. Zweng, and D. R. Johnson (2010), *World Ocean Atlas 2009*, vol. 2, *Salinity*, edited by S. Levitus, 184 pp., U.S. Govt. Print. Off., Washington, D. C.

Balaguru, K. (2011), Barrier layers of the Atlantic Warm pool: Formation mechanism and influence on weather and climate, PhD thesis, Tex. A&M Univ., College Station.

Bentamy, A., Y. Quilfen, F. Gohin, N. Grima, M. Lenaour, and J. Servain (1996), Determination and validation of average wind fields from ERS-1 scatterometer measurements, *Global Atmos. Ocean Syst.*, *4*, 1–29.

Berliand, M. E., and T. G. Strokina (1980), Global distribution of the total amount of clouds, technical report, 71 pp., Hydrometeorol. Publ. House, Saint Petersburg, Russia.

Blanke, B., and P. Delecluse (1993), Variability of the tropical Atlantic Ocean simulated by a general circulation model with two different mixed-layer physics, *J. Phys. Oceanogr.*, *23*, 1363–1388.

Chen, L. G. (1995), Mixed layer density ratio from the Levitus data, *J. Phys. Oceanogr.*, *25*(4), 691–701.

de Boyer Montégut, C., G. Madec, A. S. Fisher, A. Lazar, and D. Iudicone (2004), Mixed layer depth over the global ocean: An examination of profile data and a profile-based climatology, *J. Geophys. Res.*, *109*, C12003, doi:10.1029/2004JC002378.

de Boyer Montégut, C., J. Mignot, A. Lazar, and S. Cravatte (2007a), Control of salinity on the mixed layer depth in the world ocean. Part I: General description, *J. Geophys. Res.*, *112*, C06011, doi:10.1029/2006JC003953.

de Boyer Montégut, C., J. Vialard, S. S. C. Shenoi, D. Shankar, F. Durand, C. Ethé, and G. Madec (2007b), Simulated seasonal and interannual variability of mixed layer heat budget in the northern Indian Ocean, *J. Clim.*, *20*, 3249–3268.

Dessier, A., and J. R. Donguy (1994), The sea surface salinity in the tropical Atlantic between 10°S and 30°N—Seasonal and interannual variations (1977–1989), *Deep Sea Res. I*, *41*, 81–100.

Durand, F., S. R. Shetye, J. Vialard, D. Shankar, S. S. C. Shenoi, C. Ethe, and G. Madec (2004), Impact of temperature inversions on SST evolution in the South-Eastern Arabian Sea during the pre-summer monsoon season, *Geophys. Res. Lett.*, *31*, L01305, doi:10.1029/2003GL018906.

Durand, F., D. Shankar, C. de Boyer Montégut, S. S. C. Shenoi, B. Blanke, and G. Madec (2007), Modeling the barrier-layer formation in the South-Eastern Arabian Sea, *J. Clim.*, *20*, 2109–2120.

Enfield, D. B., and L. Cid-Serrano (2010), Secular and multidecadal warmings in the North Atlantic and their relationships with major hurricane activity, *Int. J. Climatol.*, *30*(2), 174–184.

Ferry, N., and G. Reverdin (2004), Sea surface salinity interannual variability in the western tropical Atlantic: An ocean general circulation model study, *J. Geophys. Res.*, *109*, C05026, doi:10.1029/2003JC002122.

Foltz, G. R., and M. J. McPhaden (2008), Seasonal mixed layer salinity balance of the tropical North Atlantic Ocean, *J. Geophys. Res.*, *113*, C02013, doi:10.1029/2007JC004178.

Gent, P. R., and J. C. McWilliams (1990), Isopycnal mixing in ocean circulation models, *J. Phys. Oceanogr.*, *20*, 150–151.

Giannini, A., Y. Kushnir, and M. C. Cane (2000), Interannual variability of Caribbean rainfall, ENSO, and the Atlantic Ocean, *J. Clim.*, *13*, 297–310.

Jacket, D. R., and T. J. McDougall (1995), Minimal adjustment of hydrographic data to achieve static stability, *J. Atmos. Oceanic Technol.*, *12*, 381–389.

Jerlov, N. G. (1968), *Optical Oceanography*, 194 pp., Elsevier, Amsterdam.

Kalnay, E., et al. (1996), The NCEP/NCAR 40-year reanalysis project, *Bull. Am. Meteorol. Soc.*, *77*, 437–471.

Knight, J. R., R. J. Allan, C. K. Folland, M. Vellinga, and M. E. Mann (2005), A signature of persistent natural thermohaline circulation cycles in observed climate, *Geophys. Res. Lett.*, *32*, L20708, doi:10.1029/2005GL024233.

Levitus, S. (1998), Climatological atlas of the world ocean, *Tech. Rep., 13*, NOAA, Rockville, Md.

Liu, H., S. A. Grodsky, and J. A. Carton (2009), Observed sub seasonal variability of oceanic barrier and compensated layers, *J. Clim.*, *22*(22), 6104–6119.

Locarnini, R. A., A. V. Mishonov, J. I. Antonov, T. P. Boyer, H. E. Garcia, O. K. Baranova, M. M. Zweng, and D. R. Johnson (2010), *World Ocean Atlas 2009*, vol. 1, *Temperature*, edited by S. Levitus, 184 pp., U.S. Govt. Print. Off., Washington, D. C.

Madec, G., and M. Imbard (1996), A global ocean mesh to overcome the North Pole singularity, *Clim. Dyn.*, *12*(6), 381–388.

Madec, G., P. Delecluse, M. Imbard, and M. Levy (1998), OPA 8.1: Ocean general circulation model reference manual, *Notes du Pole de Model.*, *11*, Inst. Pierre-Simon Laplace, Paris.

Masson, S., and P. Delecluse (2001), Influence of the Amazon River runoff on the tropical Atlantic, *Phys. Chem. Earth B*, *26*(2), 137–142.

Merryfield, W. J., G. Holloway, and A. E. Gargett (1999), A global ocean model with double-diffusive mixing, *J. Phys. Oceanogr.*, *29*(6), 1124–1142.

Mignot, J., C. de Boyer Montégut, A. Lazar, and S. Cravatte (2007), Control of salinity on the mixed layer depth in the world ocean: 2. Tropical areas, *J. Geophys. Res.*, *112*, C10010, doi:10.1029/2006JC003954.

Mignot, J., C. de Boyer Montégut, and M. Tomczak (2009), On the porosity of barrier layers, *Ocean Sci.*, *5*, 379–387.

Murray, R. J. (1996), Explicit generation of orthogonal grids for ocean models, *J. Comput. Phys.*, *126*, 251–273.

Pailler, K., B. Bourles, and Y. Gouriou (1999), The barrier layer in the western tropical Atlantic Ocean, *Geophys. Res. Lett.*, *26*, 2069–2072.

Paulson, C. A., and J. J. Simpson (1977), Irradiance measurements in the upper ocean, *J. Phys. Oceanogr.*, *7*, 952–956.

Roullet, G., and G. Madec (2000), Salt conservation, free surface and varying volume: A new formulation for ocean GCMs, *J. Geophys. Res.*, *105*, 23,927–23,942.

Rudnick, D. L., and J. P. Martin (2002), On the horizontal density ratio in the upper ocean, *Dyn. Atmos. Oceans*, *36*, 3–21.

Smith, W. H. F., and D. T. Sandwell (1997), Global sea floor topography from satellite altimetry and ship depth soundings, *Science*, *277*, 1956–1962.

Smyth, W. D., D. Hebert, and J. N. Moum (1996), Local ocean response to a multiphase westerly wind burst: 2. Thermal and freshwater responses, *J. Geophys. Res.*, *101*, 22,513–22,534.

Timmermann, R., H. Goosse, G. Madec, T. Fichefet, C. Ethe, and V. Duliere (2005), On the representation of high latitude processes in the ORCA-LIM global coupled sea ice–ocean model, *Ocean Modell.*, *8*, 175–201.

Trenberth, K. E., J. G. Olson, and W. G. Large (1989), A global ocean wind stress climatology based on the ECMWF analyses, technical report, 93 pp., Natl. Cent. for Atmos. Res., Boulder, Colo.

United Nations Educational, Scientific and Cultural Organization (UNESCO) (1996), Monthly and annual discharges recorded at various selected stations, technical report, 600 pp., Paris.

Vialard, J., and P. Delecluse (1998), An OGCM study for the TOGA decade. Part I: Role of salinity in the physics of the western Pacific fresh pool, *J. Phys. Oceanogr.*, *28*, 1071–1088.

Wang, C., and D. B. Enfield (2003), A further study of the influences of the tropical Western Hemisphere warm pool, *J. Clim.*, *16*, 1476–1493.

Wang, C., D. B. Enfield, S.-K. Lee, and C. W. Landsea (2006), Influences of the Atlantic warm pool on Western Hemisphere summer rainfall and Atlantic hurricanes, *J. Clim.*, *19*, 3011–3028.

Wang, C., S.-K. Lee, and D. B. Enfield (2008a), Atlantic Warm Pool acting as a link between Atlantic Multidecadal Oscillation and Atlantic tropical cyclone activity, *Geochem. Geophys. Geosyst.*, *9*, Q05V03, doi:10.1029/2007GC001809.

Wang, C., D. B. Enfield, and S.-K. Lee (2008b), Climate response to anomalously large and small Atlantic warm pools during the summer, *J. Clim.*, *21*, 2437–2450.

Xie, P., and P. A. Arkins (1997), A 17-year monthly analysis based on gauge observations, satellite estimates and numerical model outputs, *Bull. Am. Meteorol. Soc.*, *78*(11), 2539–2558.

M. Lacarra, A. Lazar, and J. Mignot, LOCEAN, UPMC Case 100, 4 place Jussieu, F-75252 Paris CEDEX 05, France. (juliette.mignot@locean-ipsl.upmc.fr)